CHAPTER – 4

Investigation of dielectric and magnetic properties of $CaCu_{3-X}Mn_XTi_{4-X}Mn_XO_{12}$ (X = 0.10) nano-ceramic synthesized through semi-wet route

4.1 Introduction

Materials show simultaneously dielectric(Amaral et al. 2014a),(Yadava et al. 2017)and magnetic(Dias et al. 2019),(Ali et al. 2017) properties have been a great interest to modern science and technology not only the perspective of solid-state physics but also because of their potential application in microelectronic devices and systems. In recent years, the investigation of high-speed digital electronics, wireless communication, industrial demands, medical and associated increasing contact to microwave necessities to the development of effective, condensed and economically absorbed of electromagnetic energy to electromagnetic compatibility and ecofriendly in a wide frequency range.(Pandey and Mandal 2019),(Kumar et al. 2020b),(Wolska et al. 1997),(Chen et al. 2016),(Amaral et al. 2010)The multiferroic material has a high capacity to retain a unique combination of dielectric permittivity and has a very low tangent loss. The multiferroic materials show spontaneous magnetization takes place. The synthesis of magnetic material cheap synthesis and extremely low d.c. conductivity which makes them fascinating for the development of wideband microwave absorbers. The development of polymeric material and metal oxide of composite powder is how to control the frequency dispersion of complex permeability and permittivity of the composite. It is mainly obtained by the variation of composite filler types,size and shape of the host.The distribution of composite can be varied by the concentration of mixtures. There are several attempts to make control magnetic and dielectric properties of the material by different routes such as chemical vapour deposition, hydrothermal, physical vapour deposition (PVD), electrospinning method and coprecipitation. The semi-wet route is a cheap low cast useful method for obtaining accurate structural of the material at the ionic level. Semi –wet route is more homogeneity of material at the nanoscale. Researchers have performed the challenge of finding radar frequency absorbing material with a wide frequency range. Material based on hexaferrite can not full fill those

demands. The hexaferrite materials were explored resonant frequency and new system of composite powder including hard and soft material have been developed such as $SrFe_{12}O_{19}$, Fe_2O_3, $CoFe_2O_4$, $BaFe_{12}O_{19}$, Fe_3O_{12} .Mn-doped CCTO nano-ceramic must have a variety of potential applications such as catalyst, ion filter, electrochemical capacitor, electrode material batteries.(Slimani et al. 2018),(Nigam and Pawar 2020),(Ghanbari Shohany and Khorsand Zak 2020),(Ogloblichev et al. 2018 p. 2),(Asiri et al. 2018) Material which is manganese doped, useful nanoparticle and usable for processing physical and chemical properties which is strongly dependent upon morphology and nanostructure of Mn-doped electroceramics. The $CaCu_3Ti_4O_{12}$ (CCTO) has been showing giant dielectric properties. The CCTO ceramic is unlucky that the tangent loss was recorded previously very high, due to this region not suitable for capacitor application.(Almeida et al. 2009) It is reported in many research papers that when doping of homo or heteroatom into the copper or titanium site most of the studies have shown demerit that mostly maintains particular properties and other properties degrade.(Rani et al. 2018),(Liu et al. 2011),(Löhnert et al. 2015)In the previously reported research paper the cation and anion doped such as Zn^{+2}, Gd^{+3}, Sn^{+4}, Nb^{+4}, Sr^{+2}, La^{+3}, Ni^{+2}, Mg^{+2}, and F^{-1}. In the previously reported research paper when Mg^{2+} doped at the copper site , due to smaller size less agglomeration of chages inside the grain boundary take place so the dielectric constant get decreases , by doping of small cation tangent loss also decreases Mg^{2+}.(Singh et al. 2014),(Kumar et al. 2020b)

In this study, for the synthesis of $CaCu_{2.9}Mn_{0.1}Ti_{3.90}Mn_{0.1}O_{12}$ (CCMTMO) followed by the semi-wet route. The semi-wet route is very cheap for synthesizing Mn-doped CCTO ceramic in which low-cost titanium oxide used. The single-phase formation of CCMTMO ceramic was to be examined by the XRD pattern.

4.2 EXPERIMENTAL SECTION

Synthesis of material.

For the synthesis of $CaCu_{2.90}Mn_{0.10}Ti_{3.90}Mn_{0.10}O_{12}$ (CCMTMO) ceramic, semi –the wet route was followed. The starting materials were taken in the stoichiometric amount suich as Calcium nitrate tetra hydrates ($Ca(NO_3)_2.4H_2O$ (98% Merck, India)). Copper nitrate hex hydrates ($Cu(NO_3)_2.6H_2O$ Pure 99% Merck, India), Manganese acetates hydrates, $C_4H_4MnO_4.H_2O$ (Aldrich 99 % Pure) and low-cost solid Titanium oxide (TiO_2(98% Merck, India).All metal complexes were mixed in double-distilled water in the beaker for the preparation of CCMTMO ceramic. The glycine was used as a chelating agent. The color mixed complexes solution was blue, follow this solution allowed to magnetically stirred and maintain the temperature 70℃ to 80 ℃ for 12 to 15 h for the removal of water, and polyaesterification takes place. After the polyaesterification the remaining quantity was dehydrated to fully evaporation takes place. The compound was ground using mortar pestle. The compound was black, solid and crystalline. The ceramic material was calcined 600 ℃ for 12 h. The calcined powder was follow on pillarization by using polyvinyl alcohol (PVA 2 wt. %) used as the binder. The binder was burned out 500℃ for 2 h. The pellets were sintered 900℃ for 12 h.

Characterization

The thermal behavior of CCMTMO ceramic was studied by thermogravimetric analysis (TGA). The phase formation was examined by X-ray diffraction (XRD) pattern. The sample was characterized by Fourier Transform- Infrared spectroscopy (FT-IR) and Raman studied. The microstructural structural studies were performed through HR-SEM and HR-TEM. The stoichiometric of ceramic was to be confirmed by Energy

Disperse X-ray. The oxidation state was confirmed by X-ray photoelectron spectroscopy (XPS). The magnetic, dielectric, impedance and modulus spectroscopic of material also studies.

4.3. Results and discussions

Thermogravimetric (TGA) analysis

Figure 4.1 shows the TGA graph of CCMTMO ceramic. From the figure 4.1, it is clear that minor weight gian was observed at 400℃ due to the formation of intermediate compound. It is observed that there is a weight loss from 500℃ to 650 ℃ which is duedue to releasing a large amount of gases such as H_2O, CO_2 and N_2.(de Oliveira et al. 2016) The weight loss occurred at above 500℃ due to releasing of glycine and nitrate mainly which is reported in previously reported research paper.(Sharma et al. 2014) It is recorded from the plotted graph that at above 900℃ there is no further weight loss occurred, which indicates the phase formation of CCMTMO ceramic. (Sharma et al. 2014),(Kumar et al. 2020a)

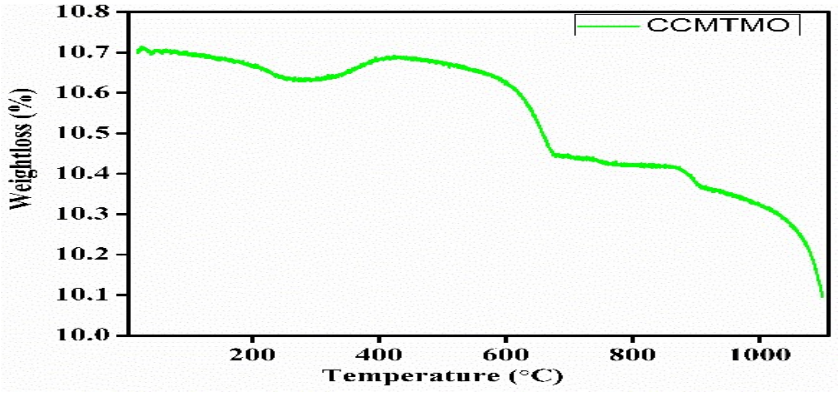

Figure 4.1. TGA plot of dry powder ($CaCu_{2.9}Mn_{0.1}Ti_{3.9}Mn_{0.1}O_{12}$ (CCMTMO) as-prepared powder .

Fourier Transform- Infrared spectroscopy (FT-IR) studies

Figure 2 shows FT-IR spectra of CCMTMO ceramic. The absorption peak at 547 cm^{-1} may be due to the bending mode of copper oxide (CuO).The peak recorded at 401 cm^{-1} is mainly due to the presence of calcium oxide bond (Ca-O).(Singh et al. 2014) It is also observed that the absorption peak recorded at 488 cm^{-1} may be Ti-O-Ti and Mn-O-Mn mixed vibration mode. In the FT-IR study, the absorption band lies in the region 300 $cm^{-1}$to 700 cm^{-1} arises from the mixed vibration of CuO_4 or MnO_4 and TiO_6 or MnO6 of CCMTMO ceramic.(Singh et al. 2014)

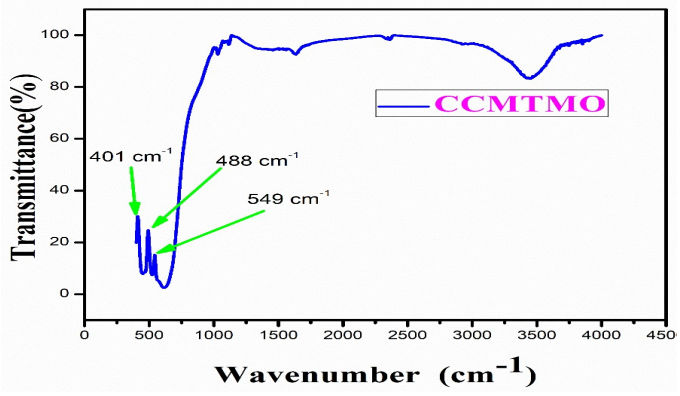

Figure 4.2. FT-IR spectra of CCMTMO ceramic sintered 900°C for 12 h.

X-ray diffraction (XRD) pattern

Figure3 shows XRD pattern of CCMTMO ceramic sintered at 900℃ for 12 h. In the displaying graph of CCMTMO ceramic, all the peaks were indexed with the help of JCPDS No. 75-2188. The perovskite system is a body-centered cubic structure of CCMTMO ceramic.(Pandey et al. 2020) It is obvious that from the recorded with the help of JCPDS card single phase formation takes place. The crystallite size of CCMTMO ceramic was be calculated Scherer's equation

$$D = \frac{k\lambda}{\beta \cos\theta} \ldots\ldots\ldots \quad (1)$$

In the above equation (1)k is crystal shape coefficient (k = 0.89,), λ represents the wavelength (1.54 Å) of the X-ray, β represents the full-width half maxima (FWHM) and θ is Braggs diffraction angle. The value of the crystallite size of CCMTMO was observed 39.5 nm. In our previously reported research paper the crystallite size was observed 52.39 nm .(Kumar et al. 2020b) When Mn doped in the CCTO ceramic the crystallite size decreases.CCTO has a cubic structure with a lattice constant a=7.36 ˚A .The analysis of X-ray diffraction of CCMTMO with Lebail refinement using FULLPROF suite software gives the following lattice parameter. The lattice constant of cubic CCMTMO was found to be 7.3940 Å.(Si et al. 2002),(Han et al. 2017)

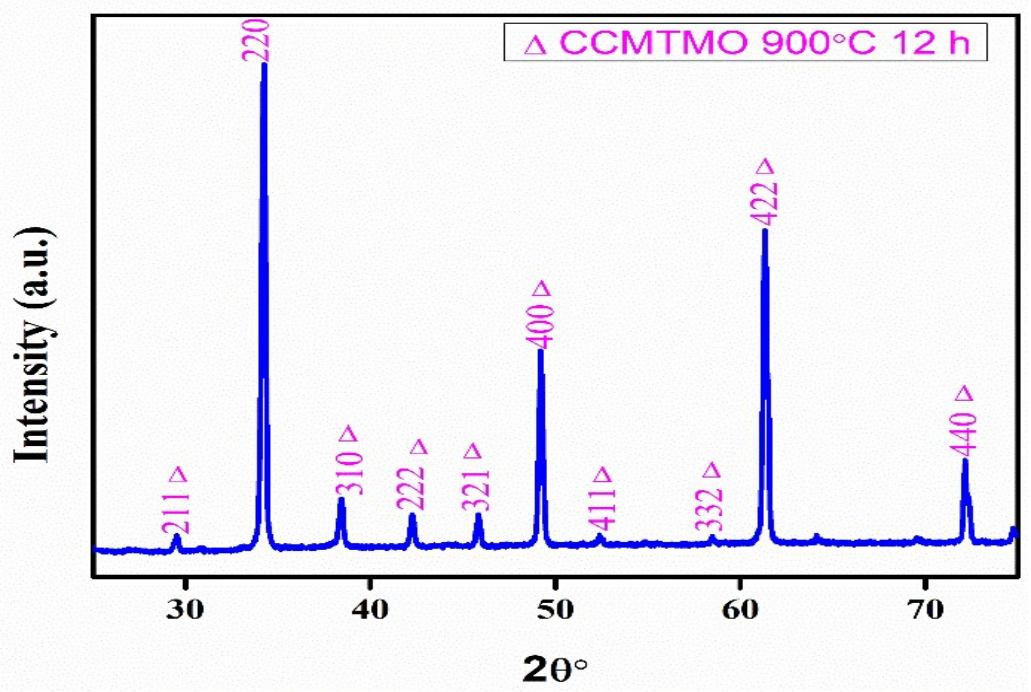

Figure 4.3.displays the XRD patterns of the sintered CCMTMO ceramic sintered at 900°C for 12 h.

Raman Sudies

Figure 4 depicts the Raman spectra of CCMTMO ceramic sintered at 900°C for 12 h. The scattered peak (Raman Shift) observed at 369 cm^{-1} highest intensity peaks and Raman shift observed at 843 cm^{-1} lowest intensity peak which suggests to the phase formation of CCMTMO ceramic. The Raman shift occurred at 369 cm^{-1} mainly evidence of the presence of copper oxide (CuO) present in the grain boundary of CCMTMO ceramic.It is observed from the showing graph two types of intensity of peak recorded at 369 cm^{-1},717 cm^{-1} highest and 426 cm^{-1},497 cm^{-1},660 cm^{-1}, 660 cm^{-1},843 cm^{-1}. Raman shift recorded at 369 cm^{-1}evidance the existence of Eg symmetry. Raman shift that occurred at 497 cm^{-1} and 660 cm^{-1} resilient to the associated with the A_1g symmetry and octahedral rotation takes place. The scattered peak found at 606 cm^{-1} is associated with the Fg symmetry. The Fg symmetry is related to Mn-O-Mn or Ti-O-

Ti anti stretching.The highest Raman shift occurred at 717 cm^{-1} and 843 cm^{-1}could be the first principal calculation at 843 cm^{-1}may be symmetrical stretching mode of Mn-O.The peak recorded at 369 cm^{-1}, 426 $cm^{-1}$and 717 cm^{-1},843 cm^{-1}mainly represent of copper oxide (CuO) and manganese oxide (MnO) bond in the grain boundary.The spectral line observed at 369 cm^{-1} associated and justified the presence of copper oxide in the grain boundary.The Raman active mode A_2g already reported previous research paper .(Singh et al. 2014)

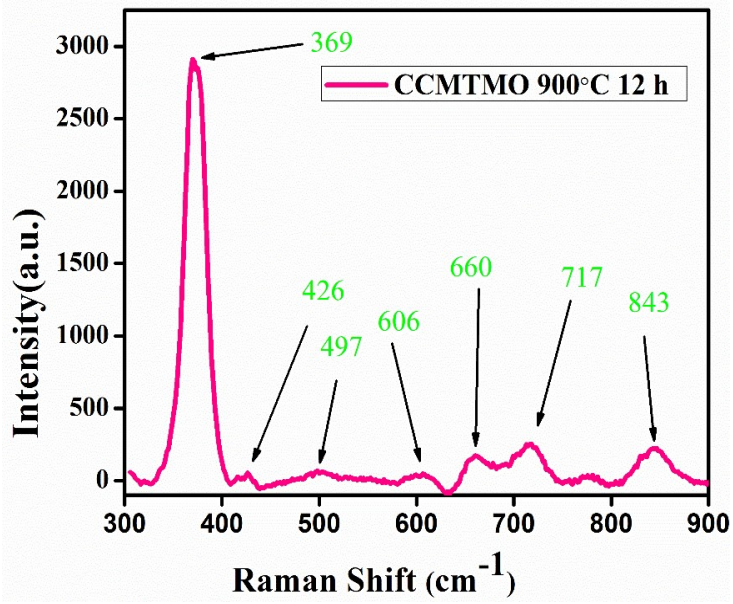

Figure 4.4.displays the Raman shift of CCMTMO ceramic sintered at 900°C for 12 h.

4.3.1Microstructural Studied

High Resolution -Scanning Electron Microscopic (HR-SEM) studies

Figure 5 shows the morphology and microstructural picture of CCMTMO ceramic.It pointed out that the grain and grain boundary well separated. The graph of CCMTMO ceramic look like in cubical structure.The grain size of CCMTMO ceramic was to be

measured by using Image j software . It is observed that from the HR-SEM graph the average grain size was found 537.62 nm. The grain of CCMTMO ceramic well dandified.The densification of grainsare mainly responsible for conductivity properties.

Energy disperse X-ray analysis (EDX)

It is displayed from the EDX spectrum of CCMTMO ceramic sintered at 900℃ for 12 h. Figure 5 (b) shows the atomic percentage of ceramic such as calcium (Ca), copper (Cu), manganese (Mn), titanium (Ti). and oxygen (O) were present in their stoichiometric ratio 6.07,17.79 1.39, 21.98 and 52.76, respectively. In the EDX spectrum all elemental composition were present in their specific color. It is observed that all the distribution of elements in homogeneous and heterogeneous in different areas.

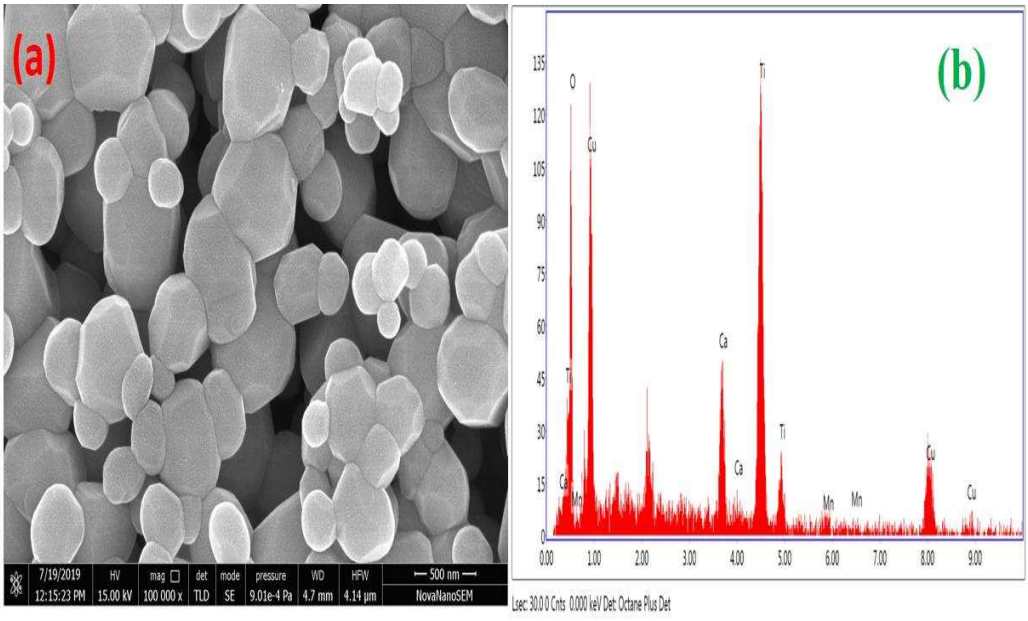

Figure 4.5.(a) displays the morphology and microstructure of sintered CCMTMO ceramic and (b) displays Energy Disperse X-ray (EDX) .

High-resolution Transmission Electron Microscopic study (HR-TEM)

Figure 6 (a) indicates the graph of sintered CCMTMO ceramic. It is observed from the bright field TEM image all particle are seeing cubical shape. The measurement of particle size was to be performed by image –j software. The average particle size was observed 0.5µm (500 nm) which indicates the nature of particles are in the range nanocrystalline. figure 6 (b) shows that the SEAD pattern of CCMTMO ceramic. It is observed that from the SEAD pattern the ring-like spot was found which shows the body-centered structure of the ceramic. This data also supported by the XRD, HR-SEM, FT-IR.

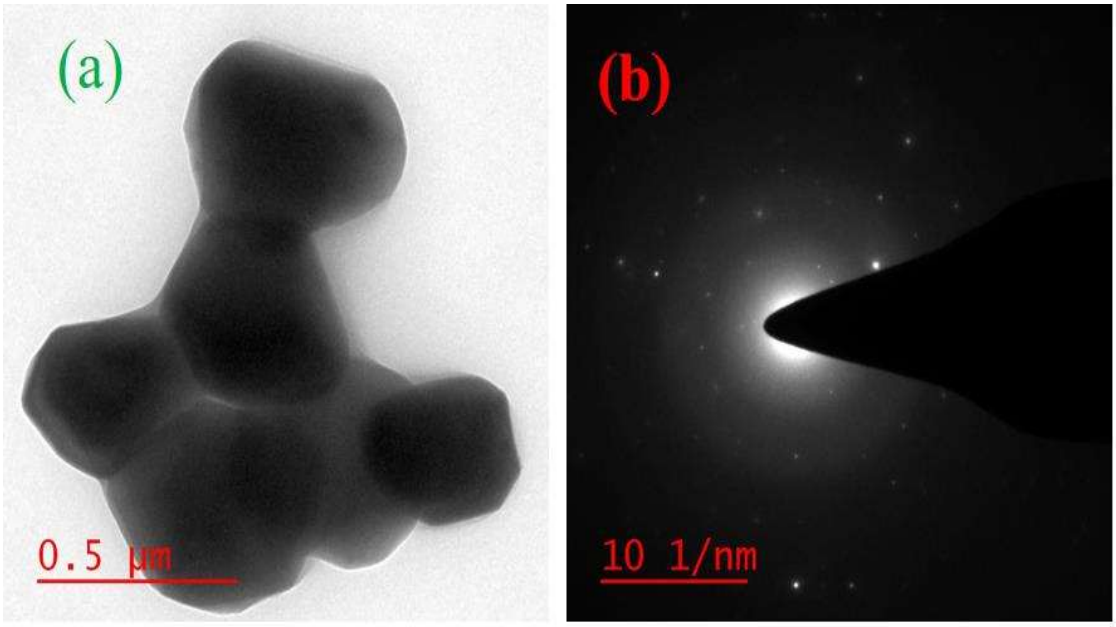

Figure 4.6 (a) displays the HR-TEM image of sintered CCMTMO ceramic (b) displays the SEAD pattern.

X-ray Photoelectron Spectroscopic (XPS) studies

Figure 7 (a to e) displays the XPS spectrum of calcium (Ca) , copper (Cu), manganese (Mn), titanium (Ti) and oxygen (O) . In many research papers it is mentioned that the X-ray photoelectron spectroscopy is a sensitive instrument for the detection of the oxidation state of individual elements present in the complex

compound. It is observed that for the reference which has given value 284 electron volt (eV) of carbon was taken to compensate the surface of charge effect. The metal cation in the CCMTMO ceramic were present in their required oxidation state. The anion (Oxygen) also present in the required oxidation state. The fitting of XPS and background deduction was to be performed with the using software XPS –Peak 4.1. Figure 7 (a) depicts the XPS spectrum of calcium , the peaks were recorded at 346.6 eV and 350.6 eV, the ground state term symbol of these two peaks $^2p_{3/2}$ and $^2p_{1/2}$ respectively. These two peaks recorded proving that calcium present in the +2 oxidation state. Figure 7 (b) depicts the XPS spectrum of copper, it noted from the plotted graph that binding energy of peaks was to be recorded at 934.1 eV and 954.2 eV proving that the existence of copper (Cu 2P spectra) in +2 oxidation state, the ground state term symbol was to be recorded Cu $^2p_{3/2}$ and Cu $^2p_{1/2}$ respectively. In this spectrum,satellite peak also recorded.(Ghodselahi et al. 2008)

It is observed from Figure 7 (C) the XPS spectrum of (at the at the 2 P lavel) manganese, which is present in the CCMTMO ceramic. The binding energy peaks were to be recorded at 641.3 eV,653.4 eV and 643.8 eV. The ground state term symbol of the deconvoluted peaks of Mn $^2p_{3/2}$ and Mn $^2p_{1/2}$ mainly related to the 641.3 eV and 653.4 eV, respectively.The peaks which are showing splitting due to spin-orbital coupling. Figure 7 (d) depicts the plotted graph of titanium (Ti 2P lavel) . It is observed from the plotted that the binding energy peak recorded at 458.1 eV , 463.6 eV, the ground state term symbol of these two peaks Ti $^2p_{3/2}$ and Ti ^{2}p1/2 doublet respectively.From the above discussion it is proving that titanium exists +4 oxidation state .Figure 7 (e) depicts the XPS spectrum of oxygen (at 1S level). The binding energy peak recorded at 529 eV, 531 eV. The peak which is recorded at 929 eV slightly asymmetric type of 1s level.(Kumar et al. 2020a),(Jaiswar and Mandal 2017),(Ghodselahi et al. 2008)

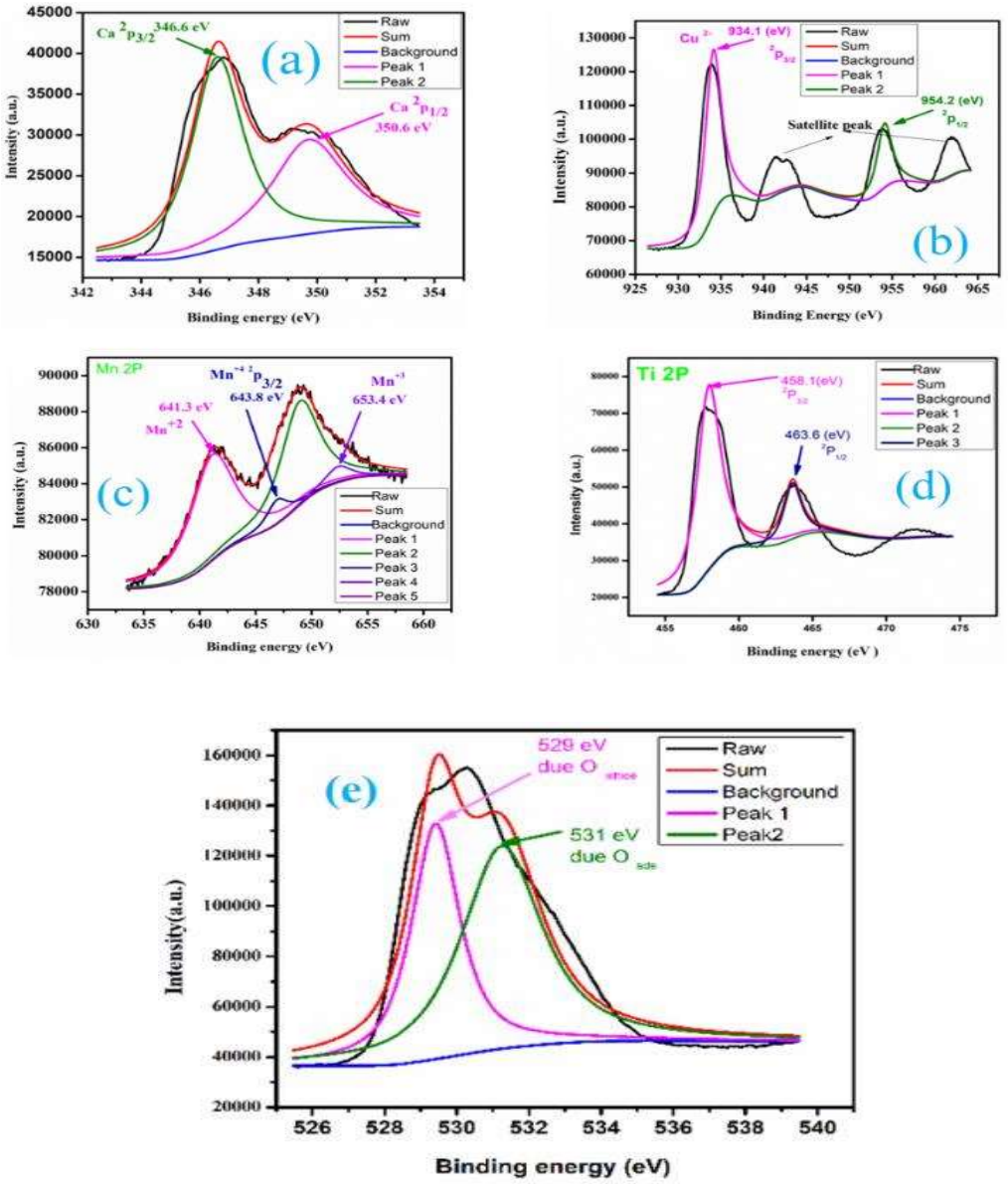

Figure 4.7. (a) to (e) display the XPS spectrum of Ca,Cu,Mn,Ti and oxygen respectively.

4.3.2 Magnetic property studies

Figure 8 (a) displays the magnetization (emu/g) versus magnetic field. It was recorded in the range between ± 60 kOe at 300 K (main panel) and 5 K (inset figure). It is observed from the plotted graph that the CCMTMO complex perovskite behave weak ferromagnetic character. It is observed from the plotted graph that the CCMTMO ceramic zero coercivity at the 300 K.It clear from the recorded graph that the magnetization curve does not saturation take place at even 60 kOe field obvious non-colinear spin arrangement. The CCMTMO complex perovskite shows the ferromagnetism character. In the complex perovskite system copper present in Cu^{2+} (S = $1/_2$) spins).In the previously reported research paper, the CCTO ceramic shows the paramagnetic character. The magnetic properties of Mn-doped CCTO ceramic more magnetic character and behave like a ferromagnetic character. It is observed that the CCMTMO ceramic has zero coercivity and remanence. The CCMTMO ceramic free from magnetic anisotropy ion (Mn^{+2}).From the above discussion, the magnetic anisotropy non-collinear spin arrangement takes place.(Berry et al. 2000),(Pandey et al. 2019),(Mu et al. 2015),

Figure 8 (b) shows thermal variation of magnetization recorded in ZFC and FC state. In this characterization the external magnetic field 10 mT for the CCMTMO ceramic.It is observed from the plotted graph that the zero-field cooled (MZFC) and field-cooled (MFC) magnetization curves display the reversible thermogravimetric behavior with the classic antiferromagnetic transition at Neel temperature (T_N) recorded at 22.5 (Fig. 8 (b)). It is well known that the transition region was first time studied by Kim et al.The transition region was studied by with the help of neutron diffraction and electron paramagnetic resonance detected antiferromagnetism in the light of a double primitive cell in which each Cu-Cu nearest neighbour pair has antiparallel spins. It is observed

that when highly magnetic manganese was substituted to nonmagnetic Ti^{4+} ion (0 μB).It is pointed out that when manganese doped into the CCTO ceramic it strongly affects to antiferromagnetic transition. In the previously reported research paper,antiferromagnetic transition of $CaCu_3Ti_4O_{12}$ was recorded at 25 K (T_N)(Chenavas et al. 1975),(Ali et al. 2017),(Pal et al. 2018),(Singh et al. 2020),(Pansara et al. 2018),(Grubbs et al. 2005) but when manganese doped in the ceramic the antiferromagnetic transition recorded at 22.5 K (T_N).

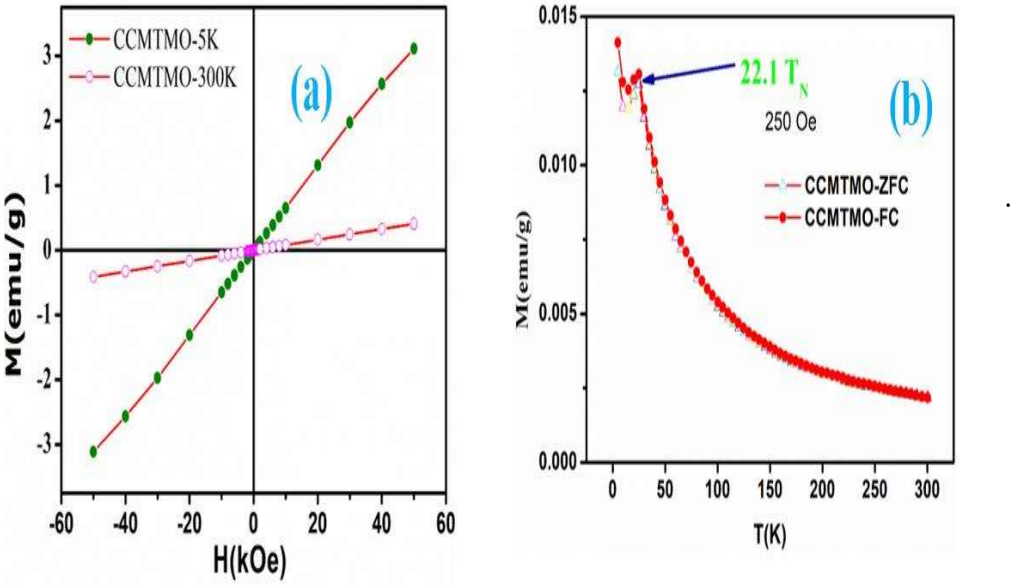

Figure 4.8. (a) displays the magnetization versus magnetic field(b) magnetization versus temperature CCMTMO.

4.3.3 Dielectric studies

Figure 4.9(a) and (b) show the variation of temperature and frequency dependant dielectric constant of CCMTMO ceramic sintered at 900 °C for 12 h.(Berry et al. 2000),(Wang et al. 2016). The dielectric constant was to be recorded at few selected temperature and frequency such as 313 K, 353 K, 393K and 10 Hz, 100 Hz, 10 kHz respectively.It is observed from the plotted graph that the value of dielectric constant exhibits a step-like behavior.(Wang et al. 2016) The value of the dielectric constant was found to be 375 and 70 concerning temperature and frequency, respectively. It is pointed out that in many research papers of Mn-doped CCTO ceramic have been studied previously reported that the dielectric constant largely decrease by doping copper site or titanium site and reported that manganese is transition metal it shows variable oxidation state. In this research paper with help of X-ray photoelectron spectroscopy (decribed in Figure 4.7 C) manganese exhibit Mn^{+2}, Mn^{+3}, Mn^{+4} oxidation state so the grain (GB) and grain boundary are behaving slightly conducting nature, so the dielectric constant largely decreases as compared to CCTO ceramic. It is observed from the plotted graph that the dielectric constant at room temperature was to be recorded 70. The dielectric constant of CCMTMO ceramic decreases with increasing frequency and temperature.(Wang et al. 2016),(Subramanian et al. 2000),(Amaral et al. 2014b),(Cai et al. 2007),(Kumar et al. 2020c)

Figure 4.9 (c) and (d) show the tangent loss of CCMTMO ceramic concerning temperature and frequency. The tangent loss of CCMTMO ceramic 0.3 and 0.4 temperature and frequency independent. It is observed at few selected temperatures and frequency such as 313 K, 353 K,393 K (temperature) and 10 Hz, 100 Hz,10 kHz

(frequency) respectively. In the previously reported research paper the tangent loss of CCTO was too high that not suitable for the capacitor application.(Almeida et al. 2009),(Liu et al. 2011) It is observed that ferroelectricity characterized by diffuse phase

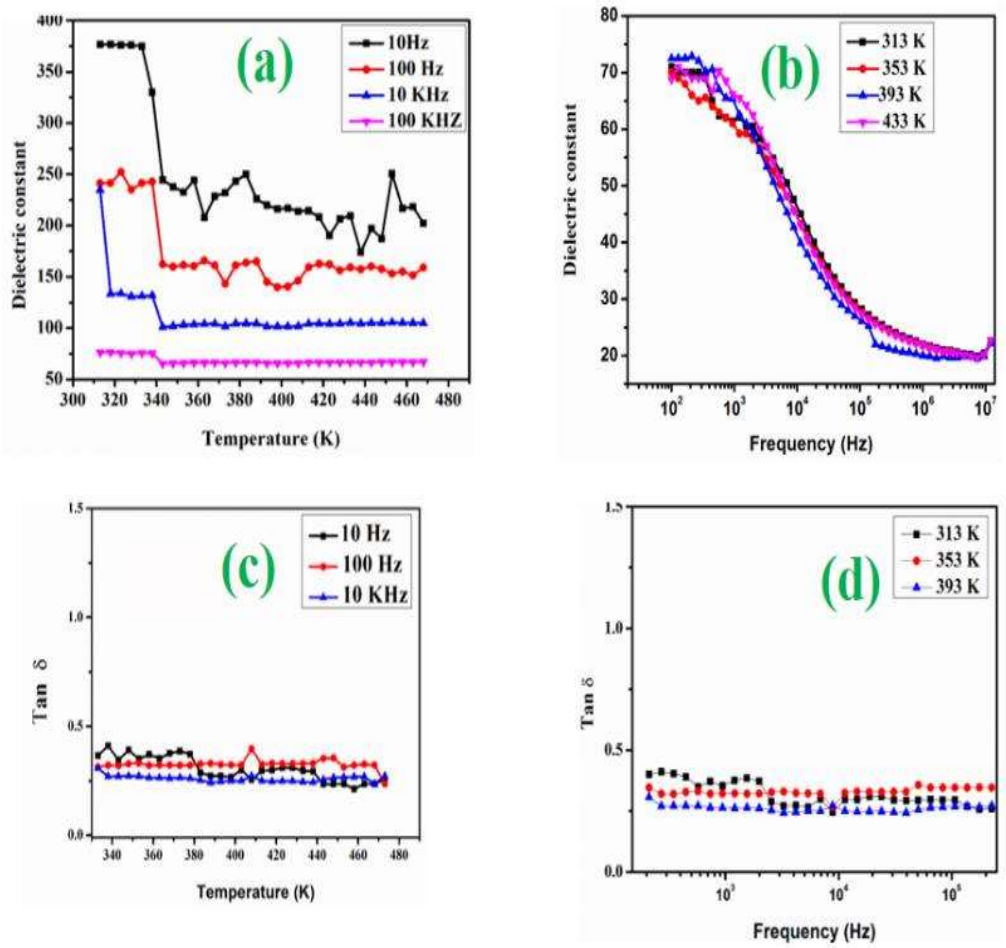

Figure 4.9 show (a) and (b) the dielectric constant of CCMTMO ceramic versus temperature and frequency, respectively. (c) and (d) depicts the tangent loss of CCMTMO ceramic versus temperature and frequency respectively.

transition and strong relaxation dispersion behavior of dielectric constant and tangent loss. It is observed from the plotted graph that the sintered CCMTMO ceramic the dielectric constant and tangent loss was to be recorded at 10 Hz. In the plotted graph at 10 Hz frequency dielectric constant and tangent loss was to observed 375 and 0.3, respectively. It is pointed out from the plotted graph of CCMTMO ceramic at room temperature the tangent loss was to be observed 0.3. It noted from the plotted graph of CCMTMO concerning temperature and frequency independent. It observed that the origin of dielectric constant is mainly due to space charge polarization by the accumulation of charge carrier interface of semiconducting grain (g) and grain boundaries (g_b).

Conclusions

The CCMTMO ceramic was successfully synthesized through semi-wet route. The crystallite size was observed 39.5 nm. The thermal behavior was studied by thermogravimetric analysis. The single phase formation was examined by XRD pattern. The metal-oxygen bond was confirmed by FT-IR spectra. Raman spectra shows evidence copper oxide (CuO) and manganese oxide (MnO) present in the grain and grain boundaries . The microstructural structural study was performed by HR-TEM and HR-SEM. The grain size and particle were observed 537.6152 nm and 0.5 μm respectively. The oxidation state of a cation such as calcium, copper, and titanium were to be observed +2,+2,+4 respectively. Manganese exhibit variable oxidation state which mainly responsible for largely decrease dielectric constant of CCMTMO ceramic. The anion present in the CCMTMO ceramic with the help of binding energy against

intensity shows -2 oxidation state. It is observed from MPMS data also support the crystalline nature of CCMTMO ceramic. The magnetization versus magnetic field graph shows zero coercivity. The antiferromagnetic transition (T_N) was to occur at 22.5 K.The dielectric constant was to be obtained 375 at 10 Hz frequence .The tangant loss of CCMTMO ceramic was to be found 0.3.The decrease in dielectric constant , manganese (Mn) shows variable oxidation state.

References

Ali, K., Bahadur, A., Jabbar, A., Iqbal, S., Ahmad, I., Bashir, M.I., 2017. Synthesis, structural, dielectric and magnetic properties of CuFe 2 O 4 /MnO 2 nanocomposites. *Journal of Magnetism and Magnetic Materials* **434**, 30–36. https://doi.org/10.1016/j.jmmm.2016.12.009

Almeida, A.F.L., Fechine, P.B.A., Graça, M.P.F., Valente, M.A., Sombra, A.S.B., 2009. Structural and electrical study of CaCu3Ti4O12 (CCTO) obtained in a new ceramic procedure. *J Mater Sci: Mater Electron* **20**, 163–170. https://doi.org/10.1007/s10854-008-9675-4

Amaral, F., Clemente, E., Valente, M.A., Costa, L., Costa, F., 2014a. Effects of Mn doping on the electrical and dielectric properties of CaCu3Ti4O12 fibres. *Ceramics International* **40**, 16503–16511. https://doi.org/10.1016/j.ceramint.2014.08.002

Amaral, F., Clemente, E., Valente, M.A., Costa, L., Costa, F., 2014b. Effects of Mn doping on the electrical and dielectric properties of CaCu3Ti4O12 fibres. *Ceramics International* **40**, 16503–16511. https://doi.org/10.1016/j.ceramint.2014.08.002

Amaral, F., Valente, M., Costa, L., 2010. Synthesis and Characterization of Calcium Copper Titanate Obtained by Ethylenediaminetetraacetic Acid Gel Combustion. *Materials Chemistry and Physics* **124**, 580–586. https://doi.org/10.1016/j.matchemphys.2010.07.016

Asiri, S., Güner, S., Demir, A., Yildiz, A., Manikandan, A., Baykal, A., 2018. Synthesis and Magnetic Characterization of Cu Substituted Barium Hexaferrites. *J Inorg Organomet Polym* **28**, 1065–1071. https://doi.org/10.1007/s10904-017-0735-1

Berry, F.J., Greaves, C., Helgason, Ö., McManus, J., Palmer, H.M., Williams, R.T., 2000. Structural and Magnetic Properties of Sn-, Ti-, and Mg-Substituted α-Fe2O3: A Study by Neutron Diffraction and Mössbauer Spectroscopy. *Journal of Solid State Chemistry* **151**, 157–162. https://doi.org/10.1006/jssc.1999.8605

Cai, J., Lin, Y.-H., Cheng, B., Nan, C.-W., He, J., Wu, Y., Chen, X., 2007. Dielectric and nonlinear electrical behaviors observed in Mn-doped CaCu3Ti4O12 ceramic. *Appl. Phys. Lett.* **91**, 252905. https://doi.org/10.1063/1.2825472

Chen, Y.-C., Liu, J.-L., Ungur, L., Liu, J., Li, Q.-W., Wang, L.-F., Ni, Z.-P., Chibotaru, L.F., Chen, X.-M., Tong, M.-L., 2016. Symmetry-Supported Magnetic Blocking at 20 K in Pentagonal Bipyramidal Dy(III) Single-Ion Magnets. *J. Am. Chem. Soc.* **138**, 2829–2837. https://doi.org/10.1021/jacs.5b13584

Chenavas, J., Joubert, J.C., Marezio, M., Bochu, B., 1975. The synthesis and crystal structure of CaCu3Mn4O12: A new ferromagnetic-perovskite-like compound. *Journal of Solid State Chemistry* **14**, 25–32. https://doi.org/10.1016/0022-4596(75)90358-8

Dias, D.F., Braga, T.P., Soares, J.M., Sasaki, J.M., Dias, D.F., Braga, T.P., Soares, J.M., Sasaki, J.M., 2019. Structural, Morphological and Magnetic Properties of FeCo-(Fe,Co)3O4 Nanocomposite Synthesized by Proteic Sol-Gel Method Using a Rotary Oven. *Materials Research* **22**. https://doi.org/10.1590/1980-5373-mr-2018-0446

Ghanbari Shohany, B., Khorsand Zak, A., 2020. Doped ZnO nanostructures with selected elements - Structural, morphology and optical properties: A review. *Ceramics International* **46**, 5507–5520. https://doi.org/10.1016/j.ceramint.2019.11.051

Ghodselahi, T., Vesaghi, M.A., Shafiekhani, A., Baghizadeh, A., Lameii, M., 2008. XPS study of the Cu@Cu2O core-shell nanoparticles. *Applied Surface Science* **255**, 2730–2734. https://doi.org/10.1016/j.apsusc.2008.08.110

Grubbs, R.K., Venturini, E.L., Clem, P.G., Richardson, J.J., Tuttle, B.A., Samara, G.A., 2005. Dielectric and magnetic properties of Fe- and Nb-doped CaCu 3 Ti 4 O 12. *Phys. Rev. B* **72**, 104111. https://doi.org/10.1103/PhysRevB.72.104111

Han, F., Ren, S., Deng, J., Yan, T., Ma, X., Peng, B., Liu, L., 2017. Dielectric response mechanism and suppressing high-frequency dielectric loss in Y2O3 grafted CaCu3Ti4O12 ceramics. *J Mater Sci: Mater Electron* **28**, 17378–17387. https://doi.org/10.1007/s10854-017-7671-2

Jaiswar, S., Mandal, K.D., 2017. Evidence of Enhanced Oxygen Vacancy Defects Inducing Ferromagnetism in Multiferroic $CaMn_7O_{12}$ Manganite with Sintering Time. *J. Phys. Chem. C* **121**, 19586–19601. https://doi.org/10.1021/acs.jpcc.7b05415

Kumar, V., Kumar, A., Kumar Verma, M., Singh, S., Pandey, S., Singh, L., Singh, N.B., Mandal, K.D., 2020a. Observation of Unusual Griffith's Phase behavior in Quadruple perovskite oxide CaCu3Mn4O12 (CCMO) Synthesized through Chemical Route. *Arabian Journal of Chemistry*. https://doi.org/10.1016/j.arabjc.2020.01.003

Kumar, V., Kumar, A., Verma, M.K., Singh, S., Pandey, S., Rai, V.S., Prajapati, D., Das, T., Singh, N.B., Mandal, K.D., 2020b. Investigation of dielectric and electrochemical behavior of CaCu3−xMnxTi4O12 (x = 0, 1) ceramic synthesized

through semi-wet route. *Materials Chemistry and Physics* 122804. https://doi.org/10.1016/j.matchemphys.2020.122804

Kumar, V., Kumar, A., Verma, M.K., Singh, S., Pandey, S., Rai, V.S., Prajapati, D., Das, T., Singh, N.B., Mandal, K.D., 2020c. Investigation of dielectric and electrochemical behavior of CaCu3−Mn Ti4O12 (x = 0, 1) ceramic synthesized through semi-wet route. *Materials Chemistry and Physics* **245**, 122804. https://doi.org/10.1016/j.matchemphys.2020.122804

Liu, Q.X., Tang, X.G., Jiang, Y.P., Dong, F.L., 2011. The Dielectric Characteristics of Sr and Mg Doped CCTO Ceramics [WWW Document]. *Materials Science Forum*. https://doi.org/10.4028/www.scientific.net/MSF.687.416

Löhnert, R., Schmidt, R., Töpfer, J., 2015. Effect of sintering conditions on microstructure and dielectric properties of CaCu3Ti4O12 (CCTO) ceramics. *J Electroceram* **34**, 241–248. https://doi.org/10.1007/s10832-015-9982-0

Mu, C., Song, Y., Wang, H., Wang, X., 2015. Room temperature magnetic and dielectric properties of cobalt doped $CaCu_3Ti_4O_{12}$ ceramics. *Journal of Applied Physics* **117**, 17B723. https://doi.org/10.1063/1.4916116

Nigam, A., Pawar, S.J., 2020. Structural, magnetic, and antimicrobial properties of zinc doped magnesium ferrite for drug delivery applications. *Ceramics International* **46**, 4058–4064. https://doi.org/10.1016/j.ceramint.2019.10.243

Ogloblichev, V.V., Smolnikov, A.G., Sadykov, A.F., Piskunov, Y.V., Gerashenko, A.P., Furukawa, Y., Kumagai, K., Yakubovsky, A.Yu., Mikhalev, K.N., Barilo, S.N., Shiryaev, S.V., Belozerov, A.S., 2018. 17O NMR study of the triangular lattice antiferromagnet CuCrO2. *Journal of Magnetism and Magnetic Materials* **458**, 1–9. https://doi.org/10.1016/j.jmmm.2018.02.080

de Oliveira, G.F., de Andrade, R.C., Trindade, M.A.G., Andrade, H.M.C., Teodoro de Carvalho, C., 2016. Thermogravimetric and spectroscopic study (TG–DTA/FT–IR) of activated carbon from the renewable biomass source Babassu. *Quim. Nova*. https://doi.org/10.21577/0100-4042.20160191

Pal, K., Dey, A., Ray, P.P., Mordvinova, N.E., Lebedev, O.I., Mandal, T.K., Seikh, M.M., Gayen, A., 2018. Synthesis, Characterization and Catalytic Activity of Quadruple Perovskite: $CaCu_{3-x}Mn_xTi_{4-x}Mn_xO_{12}$ (x =0, 0.5 and 1.0). *ChemistrySelect* **3**, 1076–1087. https://doi.org/10.1002/slct.201703034

Pandey, S., Kumar, A., Singh, N.B., Mandal, K.D., 2019. Studies on dielectric and magnetic properties of CaCu3Ti3MnO12 ceramic synthesized via semi-wet route. *J Aust Ceram Soc*. https://doi.org/10.1007/s41779-019-00427-2

Pandey, S., Kumar, V., Mandal, K.D., 2020. Studies of sintering temperature on the microstructure, magnetic and dielectric behavior of CaCu3Ti3.5Mn0.5O12 ceramic

synthesized by semi-wet route. *SN Appl. Sci.* **2**, 480. https://doi.org/10.1007/s42452-020-2282-6

Pandey, S., Mandal, K.D., 2019. Investigation of microstructure, ferroelectric and dielectric behavior of CaCu3Ti(4−x)MnxO12 perovskites synthesized through semi-wet route. *SN Appl. Sci.* **1**, 1738. https://doi.org/10.1007/s42452-019-1647-1

Pansara, P.R., Raval, P.Y., Vasoya, N.H., Dolia, S.N., Modi, K.B., 2018. Intriguing structural and magnetic properties correlation study on Fe^{3+} -substituted calcium-copper-titanate. *Phys. Chem. Chem. Phys.* **20**, 1914–1922. https://doi.org/10.1039/C7CP06681C

Rani, S., Ahlawat, N., Sangwan, K.M., Rani, S., Punia, R., Malik, J., 2018. Structural investigation and giant dielectric response of CaCu3Ti4O12 ceramic by Nd/Zr co-doping for energy storage applications. *J Mater Sci: Mater Electron* **29**, 10825–10833. https://doi.org/10.1007/s10854-018-9150-9

Sharma, S., Yadav, S.S., Singh, M.M., Mandal, K.D., 2014. Impedance spectroscopic and dielectric properties of nanosized $Y_{2/3}Cu_3Ti_4O_{12}$ ceramic. *J. Adv. Dielect.* **04**, 1450030. https://doi.org/10.1142/S2010135X14500301

Si, W., Cruz, E.M., Johnson, P.D., Barnes, P.W., Woodward, P., Ramirez, A.P., 2002. Epitaxial Thin Films of the Giant-Dielectric-Constant Material CaCu_3Ti_4O_{12} Grown by Pulsed-laser Deposition. *Appl. Phys. Lett.* **81**, 2056–2058. https://doi.org/10.1063/1.1506951

Singh, L., Kim, I.W., Sin, B.C., Mandal, K.D., Rai, U.S., Ullah, A., Chung, H., Lee, Y., 2014. Dielectric studies of a nano-crystalline $CaCu_{2.90}Zn_{0.10}Ti_4O_{12}$ electro-ceramic by one pot glycine assisted synthesis from inexpensive TiO_2 for energy storage capacitors. *RSC Adv.* **4**, 52770–52784. https://doi.org/10.1039/C4RA08915D

Singh, S., Kumar, A., Pandey, S.K., Kumar, V., Verma, M.K., Gupta, A., Mandal, K.D., 2020. Synthesis of $Bi_4Ti_3O_{12}$ -$BaTiO_3$ nanocomposite, manifesting high dielectric and unique magnetic nature applicable in heterogeneous photocatalytic activity for degradation of Rhodamine B dye. *Materials Technology* 1–16. https://doi.org/10.1080/10667857.2020.1774228

Slimani, Y., Baykal, A., Amir, Md., Tashkandi, N., Güngüneş, H., Guner, S., El Sayed, H.S., Aldakheel, F., Saleh, T.A., Manikandan, A., 2018. Substitution effect of Cr3+ on hyperfine interactions, magnetic and optical properties of Sr-hexaferrites. *Ceramics International* **44**, 15995–16004. https://doi.org/10.1016/j.ceramint.2018.06.033

Subramanian, M.A., Li, D., Duan, N., Reisner, B.A., Sleight, A.W., 2000. High Dielectric Constant in ACu3Ti4O12 and ACu3Ti3FeO12 Phases. *Journal of Solid State Chemistry* **151**, 323–325. https://doi.org/10.1006/jssc.2000.8703

Wang, C., Ni, W., Zhang, D., Sun, X., Wang, J., Li, H., Zhang, N., 2016. Dielectric properties of pure and Mn-doped CaCu3Ti4O12 ceramics over a wide temperature range. *J Electroceram* **36**, 46–57. https://doi.org/10.1007/s10832-016-0024-3

Wolska, E., Stempin, K., Krasnowska-Hobbs, O., 1997. X-ray diffraction study on the distribution of lithium ions in LiMn2O4/LiFe5O8 spinel solid solutions. *Solid State Ionics* **101–103**, 527–531. https://doi.org/10.1016/S0167-2738(97)84078-7

Yadava, S.S., Khare, A., Gautam, P., Kumar, A., Mandal, K.D., 2017. Dielectric, ferroelectric and magnetic study of iron doped hexagonal Ba4YMn3O11.5−δ (BYMO) and its dependence on temperature as well as frequency. *New J. Chem.* **41**, 4611–4617. https://doi.org/10.1039/C6NJ04071C